Hindawi
Structural Control and Health Monitoring
Volume 2023, Article ID 9278389, 21 pages
https://doi.org/10.1155/2023/9278389

Research Article

Structural Nonlinear Model Updating Based on an Improved Generative Adversarial Network

Zi-Qing Yuan,[1] Yu Xin,[1,2] Zuo-Cai Wang,[1,2,3] Ya-Jie Ding,[1] Jun Wang,[1] and Dong-Hui Wang[4]

[1]*School of Civil Engineering, Hefei University of Technology, Hefei 230009, Anhui, China*
[2]*Anhui Engineering Laboratory for Infrastructural Safety Inspection and Monitoring, Hefei 230009, Anhui, China*
[3]*Engineering Research Center of Safety-Critical Industrial Measurement and Control Technology of the Ministry of Education, Hefei 230009, China*
[4]*China Railway Major Bridge Reconnaissance & Design Institute Co., Ltd., Wuhan 430056, Hubei, China*

Correspondence should be addressed to Zuo-Cai Wang; wangzuocai@hfut.edu.cn

Received 31 October 2022; Revised 17 December 2022; Accepted 16 January 2023; Published 7 February 2023

Academic Editor: Yongchao Yang

This study proposes a novel nonlinear model updating approach based on an improved generative adversarial network (GAN). In the improved GAN, a convolutional neural network (CNN) surrogate model is added to the discriminator network to enhance the capability of the GAN to learn the complex mapping relationship between vibration responses and nonlinear model parameters. To avoid the gradient disappearance present in the traditional GAN, a combined objective function is added to the improved GAN model. In the network training process, the instantaneous amplitudes of the decomposed accelerations are extracted as input samples and the nonlinear model parameters are defined as the GAN output. When the improved GAN is trained, the trained network model is capable of estimating the nonlinear model parameters based on measured instantaneous acceleration amplitudes. To confirm the feasibility of the improved GAN for structural nonlinear model updating, a steel-concrete hybrid bridge tower subjected to seismic excitation is numerically simulated and the effects of different numbers of data points and noise levels are studied. Furthermore, the identification accuracy of the improved GAN is compared with the updated results. For experimental applications, the shake table test of a scaled steel-concrete hybrid bridge tower subjected to seismic excitations is employed to confirm the effectiveness of the proposed nonlinear model updating method. Both numerical and experimental results demonstrate that the improved GAN model is reliable and effective for the nonlinear model updating of structures subjected to seismic excitation.

1. Introduction

Finite element model is popular for predicting structural responses in civil, aerospace, and mechanical engineering. Since a structural model is usually established based on an idealized assumption of structural material properties and boundary conditions from the original engineering design, it may not accurately represent the actual behavior of an in-service structure [1, 2]. Therefore, it is necessary to update the finite element model based on measured static and dynamic responses [3, 4]. The purpose of model updating is to minimize the mismatch between the measured and model-predicted responses [5–7]. In the past decades, structural model updating has been a concern of engineers and researchers, and multiple model updating techniques such as response surface methods [8], sensitivity methods [9], substructure approaches [10], and neural network algorithms [11] have been proposed and developed.

Although the structural model updating approaches have been successfully applied for civil engineering structures, the premise of using these techniques for structural model updating is to assume that structures are linear, and that the vibration responses of these structures are assumed to be stationary [12, 13]. However, engineering structures

may perform nonlinearly during vibration, particularly under extreme loads such as earthquakes. In this case, it is not appropriate to use linear model updating approaches. Thus, to effectively evaluate the safety performance of structures subjected to extreme operational conditions, nonlinear model updating methods shall be explored.

The problem of structural nonlinear model updating was examined by Hemez and Doebling [14], and this study aims to confirm strategies implemented for test analysis correlation and inverse problem-solving of nonlinear structures using experimental data. However, the developed test analysis correlation and inversed problem solving for nonlinear structures requires to address the following issues: (1) characterization of experiment variability, (2) generation of additional or surrogate data sets that can increase experimental knowledge, and (3) selection of features that best characterize a nonlinear data set. Subsequently, in structural health monitoring (SHM), nonlinear model updating began to attract considerable attention and a series of nonlinear model updating approaches were proposed [15]. With the rapid development of SHM systems for engineering structures [16], a considerable amount of structural dynamic response data under operational conditions can be recorded by different types of sensors such as accelerometers, GPS sensors, linear displacement transducers, and strain gauges. These measured vibration data can be employed for the inversed problem-solving of nonlinear structures using vibration-based model updating techniques.

For existing vibration-based nonlinear model updating approaches, researchers directly use vibration responses as input to develop error functions and apply optimization algorithms for nonlinear parameter calibration by minimizing the mismatches of structural responses between the nonlinear model and real structures [17–19]. Although this type of approach can accurately achieve structural nonlinear model updating, the computational cost is relatively high due to the huge amounts of data points in structural dynamic responses. Recently, with an increase in the application of time-frequency analysis methods, certain investigators have proposed using the time-frequency characteristics of structural vibration responses as input for structural nonlinear model updating. For instance, Asgarieh et al. [19] used instantaneous modal parameters, including instantaneous frequencies and mode shapes, as input to develop an objection function. The proposed approach was then successfully applied for a nonlinear model updating of an infill frame structure subjected to seismic excitations. This method depends on the identified instantaneous frequency and modes. Kurt et al. [20] proposed an analysis of structural response time series in the frequency-energy domain by developing both forced and damped frequency-energy curves. Their optimal model parameters were identified by matching the frequency-energy curves of real structures and its reduced-order nonlinear model. Wang et al. [21, 22] proposed a nonlinear model updating approach based on the instantaneous characteristics of the decomposed structural dynamic response. A limited number of data points were then selected from the identified instantaneous frequencies and amplitudes of the decomposed structural dynamic responses, which were further used to develop error functions between real structures and nonlinear models. The nonlinear model updating can then be achieved by minimizing the error function of these instantaneous parameters between the measured structural responses and model predictions. Moreover, certain probabilistic model updating approaches for nonlinear structures using structural vibration responses are reported in the literature [23, 24].

Recently, machine learning approaches and technologies have been extensively developed and applied for solving complex problems [25–27]. Certain classical machine learning tools, such as artificial neural networks [28], K-nearest neighbors [29], computer vision techniques [30], and the support vector machine [31], have been used for structural damage detection and model updating in SHM. Among machine learning techniques, deep learning-based algorithms have become increasingly popular because of their strong capability for data feature extraction and nonlinear mapping relationship construction [32, 33]. According to the advantages of deep learning algorithms in data feature learning, an improved generative adversarial network (GAN) is proposed in this study for the nonlinear model updating of bridge towers subjected to seismic excitation. In the improved network, a convolutional neural network (CNN) surrogate model is added to the discriminator network. The improved network aims to enhance the capability of the GAN to learn mapping relationships between structural vibration responses and nonlinear model parameters. After performing network training, the improved GAN model is capable of identifying optimal values for nonlinear model parameters based on input data features. To confirm the feasibility of using the improved GAN for nonlinear model updating, a steel-concrete hybrid bridge tower model subjected to seismic excitation is numerically simulated, and then, the effects of different numbers of data points and noise levels are studied. The accuracy of the improved GAN is further compared with the updated results of CNN. In an experimental application, shake table testing of a scaled steel-concrete hybrid bridge tower structure is employed to confirm the effectiveness of the proposed nonlinear model updating. Both numerical and experimental results demonstrate that the improved GAN model is reliable and effective for nonlinear model updating.

The remainder of this study is organized as follows: Section 2 introduces the theoretical development of the improved GAN and the proposed nonlinear model updating method. In Section 3, numerical simulations of a steel-concrete hybrid bridge tower subjected to seismic excitation are performed to examine the feasibility and reliability of the proposed approach. To validate the effectiveness of the proposed nonlinear model updating strategy, the shake table test of a scaled steel-concrete hybrid bridge tower subjected to seismic excitation is employed, and the nonlinear model of the tested bridge tower subjected to seismic excitation is updated in Section 4. Based on the numerical simulation and

experimental results, the corresponding conclusions are provided in Section 5.

2. Theoretical Background

2.1. Basic Principle of GAN. GAN was first developed and designed by Goodfellow et al. [34] and belongs to the category of unsupervised learning algorithms. Network training can then be achieved using two neural networks, i.e., a generator (G) and a discriminator (D). While training the networks, the generator attempts to produce a sample from a latent space similar to the training data. However, the purpose of a discriminator is to differentiate between the training data and the generated samples. Figure 1 shows the basic architecture of a GAN model [35]. Samples selected from the real training data are provided to the discriminator, and the network aims to learn the characteristics of the real samples and to become more robust to discriminate between real and fake samples. During the training process, the generator attempts to learn how to generate the distribution of training data from the latent space, and these generated samples are then presented to the discriminator, which aims to cheat the discriminator by using samples similar to real data. To summarize, the GAN training process can be classified as a problem involving a min–max game between the discriminator and generator, which can then be described as a value function [34].

$$V(D,G) = E_{x\sim p(x)}[\log(D(X))] + E_{z\sim p(z)}[\log(1 - D(G(Z)))], \tag{1}$$

$$\min_G \max_D V(D,G) = \min_G \max_D \left\{E_{x\sim p(x)}[\log(D(X))] + E_{z\sim p(z)}[\log(1 - D(G(Z)))]\right\}. \tag{2}$$

In equation (2), X is the real data with a distribution $p(x)$ and Z is a latent variable with the distribution $p(z)$; the terms $E_{x\sim p(x)}[]$ and $E_{z\sim p(z)}[]$ are the expected values of the functions within the brackets; the symbol $D()$ is the probability that samples within the brackets are obtained from real data rather than from the generator, and the symbol $D(G())$ is the probability that samples within the brackets are identified as the real data rather than the fake data produced by the generator.

According to equations (1) and (2), the training processing of a traditional GAN can be concluded as follows: (1) $\min_G V(D,G)$: maximizing the probability of assigning the correct label to both training data and generated samples from the generator by training the discriminator, that is to say, training the discriminator to maximize the term $\log(D(X))$; (2) $\max_D V(D,G)$: representing the generator is required to be trained to minimize the term $\log(1 - D(G(Z)))$, which indicates that the generated samples are close enough to real data to cheat the discriminator.

2.2. Description of the Improved GAN. In this study, the GAN is used for updating structural nonlinear models because of its advantages in unsupervised learning. However, certain problems must be solved prior to using the GAN for nonlinear model updating. The limitations of a GAN model can be described as follows. (1) In a GAN model, the generator aims to develop a mapping relationship between structural responses and nonlinear model parameters, while the discriminator discriminates fake data from the generated samples by learning the data features of nonlinear parameters. However, since the samples provided to the discriminator network only comprise generated and real nonlinear parameters, structural responses are neglected in the training process of the discriminator. The discriminator network cannot provide accurate indications to calibrate the generator in the GAN training process. (2) In a traditional GAN, the parameter optimization of the generator and the discriminator depends on the loss gradient provided by the discriminator; this phenomenon may cause the vanishing gradient problem, reducing the quality of the generated samples and even leading to network training failure.

To solve the abovementioned challenges, this study proposes a novel network structure for structural nonlinear model updating based on the traditional GAN. The basic procedure for the improved GAN is as follows. (1) A combined objective function is introduced to develop the mapping relationships between the inputs and outputs of the generator network, while skip and dense connections are applied to enhance the information exchange between the network layers, thus avoiding the vanishing gradient problem in the network training process. (2) A CNN-based surrogate model is used to enhance the discriminator network to learn the mapping relationships between the structural responses and nonlinear model parameters, which is a vital step to apply to the GAN for structural nonlinear model updating.

In the improved GAN model, when a fake nonlinear parameter set, $G(z)$, generated by the generator and a real parameter set, X, are brought into the trained CNN surrogate model, corresponding structural responses under these parameter combinations can be calculated by the surrogate model. Then, these predicted structural responses are then applied as the input of the discriminator network. In practice, the dynamic responses of structures are usually recorded by a number of sensors in an SHM system predesigned and arranged by engineers. The correlations of these measured multichannel vibration data can be explained by the vibration characteristics of structures such as mode shapes and natural frequencies. Thus, using the multichannel structural vibration data as training samples for GAN can improve the training results of network structures.

The applied generator in the improved GAN is a densely connected convolutional network (DenseNet), and the development of a generator is shown in Figure 2 [36]. As shown in Figure 2, the DenseNet has three consecutive dense blocks. During generator network training, the compression layer and bottleneck layer gradually extract higher-level data features, and the most representative data features extracted from the bottleneck layer are reassembled using the stacked reshape layer for output. To extract the high-dimensional

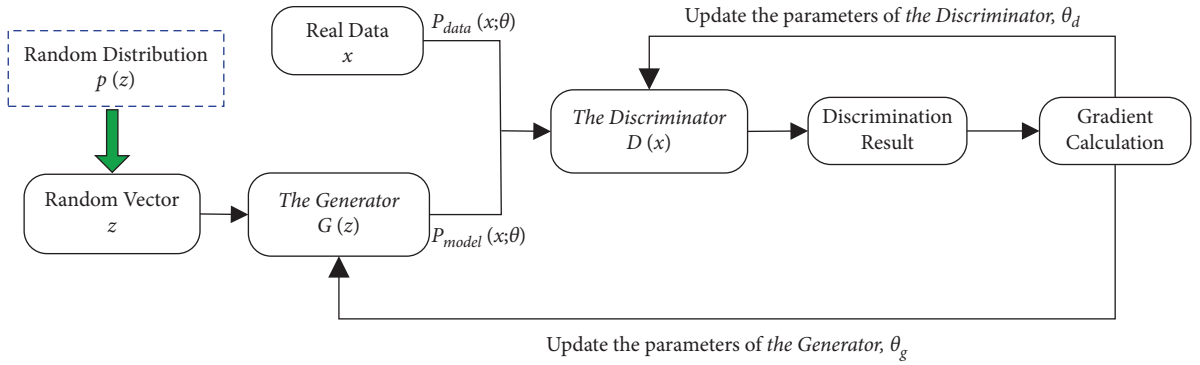

Figure 1: Basic training process of a GAN model.

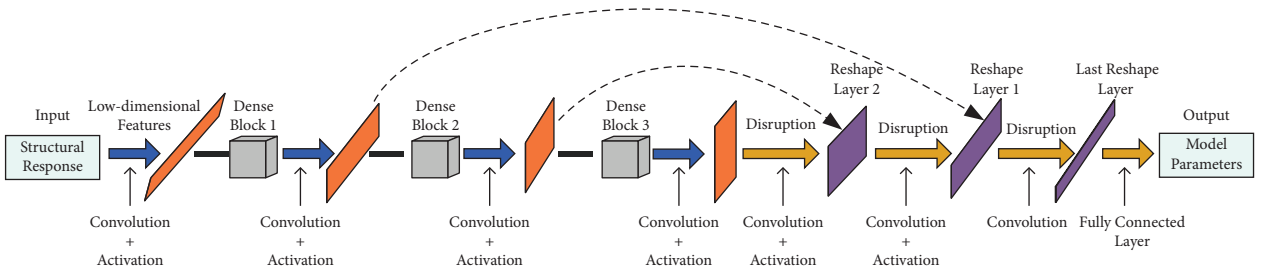

Figure 2: Construction diagram of a generator.

data features of input responses, the DenseNet substitutes typical GAN continuous convolutional layers having a dense block of three deeply connected convolutional layers, as shown in Figure 3. A dense block comprises multiple convolutional layers that use skip connections to transfer data features across layers. Because of the convolution kernel with a step size of two in the last convolutional layer, for input through dense blocks, the output feature map is reduced in size but has higher dimensional mapped features. Using the skip connection in the DenseNet generator framework, the gradient is allowed to be back-propagated directly to the shallow layers, which alleviates the gradient vanishing problem in deeper layers [37]. Moreover, the skip connection operation can reduce the requirement for training data and significantly improve the network training efficiency.

2.3. Nonlinear Model Updating Based on the Improved GAN Approach. For a nonlinear structure, the mapping relationship between the structural dynamic response, y, and its nonlinear model parameters, $\theta = (\theta_1, \theta_2, \theta_3, \ldots, \theta_k)$, can be expressed as follows:

$$\mathbf{y} = f\left(\boldsymbol{\theta} = \left(\theta_1, \theta_2, \theta_3, \ldots, \theta_k\right)\right). \tag{3}$$

In equation (3), the symbol $f()$ is a mapping function between structural responses and designed parameters, and k is the number of nonlinear model parameters.

In practice, structural dynamic responses can be directly obtained by sensors, i.e., accelerometers, linear variable differential transformers, and strain. However, real structural parameters are usually unknown because of changed operational environments and unexpected structure degradation, which inevitably causes deviation between θ and corresponding structural parameters. The deviation may result in the estimated structural responses based on the original nonlinear model not accurately matching the real structural responses. Therefore, the initial nonlinear model parameters require to be calibrated using the measured structural dynamic responses. In this study, the improved GAN model is applied to approximate the nonlinear mapping function, $f()$, defined in equation (3), and the optimal nonlinear model parameters can be directly estimated based on the trained network model. Table 1 lists the proposed structural nonlinear model updating process based on the improved GAN. In the proposed nonlinear model updating approach, the accuracy of the model updating results is significantly dependent on the learning capability of the improved GAN model.

Before the GAN network training, a CNN surrogate model is first trained to learn the mapping relationships between the structural responses and nonlinear model parameters. In this study, to construct a CNN-based surrogate model, 500 groups of nonlinear parameter combinations are used as the input of training samples, while 500 groups of the instantaneous amplitudes and instantaneous frequencies of the decomposed structural acceleration responses are used as the output. The detailed training process of a CNN model can be found in the literature [38–40]. Once training of the CNN surrogate model is completed, the trained CNN can be added to the improved GAN network, which is capable of reconstructing structural dynamic responses based on generated and real nonlinear model parameter samples. Figure 4 shows the adversarial training procedure of the improved GAN. As shown in Figure 4, the network training

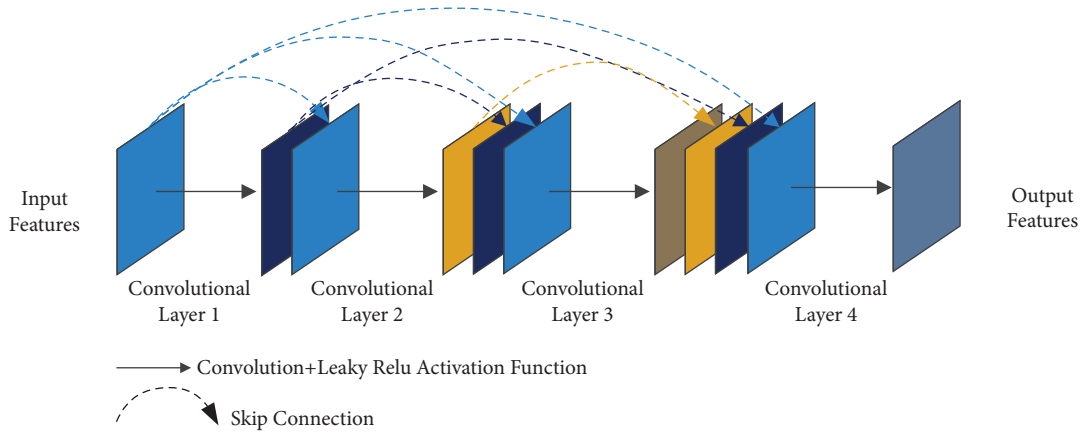

Figure 3: Network construction of a dense block.

Table 1: Nonlinear model updating process based on the improved GAN approach.

Step 1	Build the initial structural model
Step 2	Select parameters to be corrected
Step 3	Estimate the range of parameters to be corrected
Step 4	Model calculations to generate training data
Step 5	Train the GAN model
Step 6	Generalize an estimate from the real structural measured responses
Step 7	Obtain the target values of the parameters

process comprises two modules and the detailed process can be described as follows.

In the training process of the improved GAN model, assuming the obtained real training samples from the nonlinear structural model are denoted as (X_{real}, Y_{real}), Y_{real} is the simulated multichannel structural responses using the nonlinear model with parameter samples X_{real}. Then, data samples are divided into two parts denoted as (X_{train}, Y_{train}) and (X_{valid}, Y_{valid}), respectively.

In the discriminator network training process, the parameters of the generator are assumed to be fixed during the training process, and the discriminator parameters can only be adjusted by generating adversarial feedback information.

By substituting training samples of Y_{train} in the generator, it can obtain the generated nonlinear parameter samples $X_{gen} = G(Y_{trian})$. These obtained samples, X_{gen}, are then used as the input of the surrogate model, which aims to predict structural responses related to Y_{valid}. The predicted structural responses can be expressed as follows:

$$Y^*_{valid} = C_{NN}\left(X_{gen}\right) = C_{NN}\left(G\left(Y_{train}\right)\right). \tag{4}$$

Then, Y_{train} and Y^*_{valid} are integrated to become a full sample combination, $[Y_{train}, Y^*_{valid}]$, which is labeled as Y_{gen}. Y_{gen} and Y_{real} are then substituted in the discriminator for discrimination. To distinguish between the generated samples and the real data samples, a sigmoid function in the output layer of the discriminator is used to perform the regression operation [41], which is expressed as follows:

$$\text{Sigmoid}\left(x\right) = \frac{1}{1+e^{-x}}. \tag{5}$$

Finally, the discriminator can distinguish samples between Y_{gen} and Y_{real} according to the calculated loss values of the cross entropy. Moreover, the obtained loss gradient is returned to each layer of the discriminator network and the training of the discriminator is achieved.

Once the discriminator network is trained, the network parameters of the discriminator are fixed and the generator can then start to be trained.

While training the generator, Y_{train} is first considered as the input of the generator, the generated nonlinear parameter samples are then denoted as $\hat{X}_{gen} = \hat{G}(Y_{train})$, further considering the generated samples into the CNN-based surrogate model to obtain the estimated samples, $\hat{C}_{NN}(\hat{G}(Y_{train}))$. Then, Y_{train} and $\hat{C}_{NN}(\hat{G}(Y_{train}))$ are integrated to be a full sample combination, $[Y_{train}, \hat{C}_{NN}(\hat{G}(Y_{real}))]$, which is denoted as $\hat{Y}_{gen}$. The sample set $\hat{Y}_{gen}$ is then considered in the discriminator network and the cross-entropy loss between $\hat{\mathbf{Y}}_{gen}$ and Y_{real} can be calculated as follows:

$$\begin{aligned} L_{\text{GAN}} = \arg\min_{G}\max_{D}\Big\{&E_{Y_{train},Y_{valid}}\left[\log D\left(Y_{real}\right)\right] \\ &+E_{Y_{train}}\left[\log\left(1-D\left(\hat{Y}_{gen}\right)\right)\right]\Big\}. \end{aligned} \tag{6}$$

During the generator training process, a combined objective function is developed for network parameter training to improve the learning ability of the improved GAN for low-frequency data features and can be expressed as follows:

$$L_{\text{IGAN}} = L_{\text{GAN}} + \lambda L_{X-\text{distance}} + \beta L_{Y-\text{distance}}. \tag{7}$$

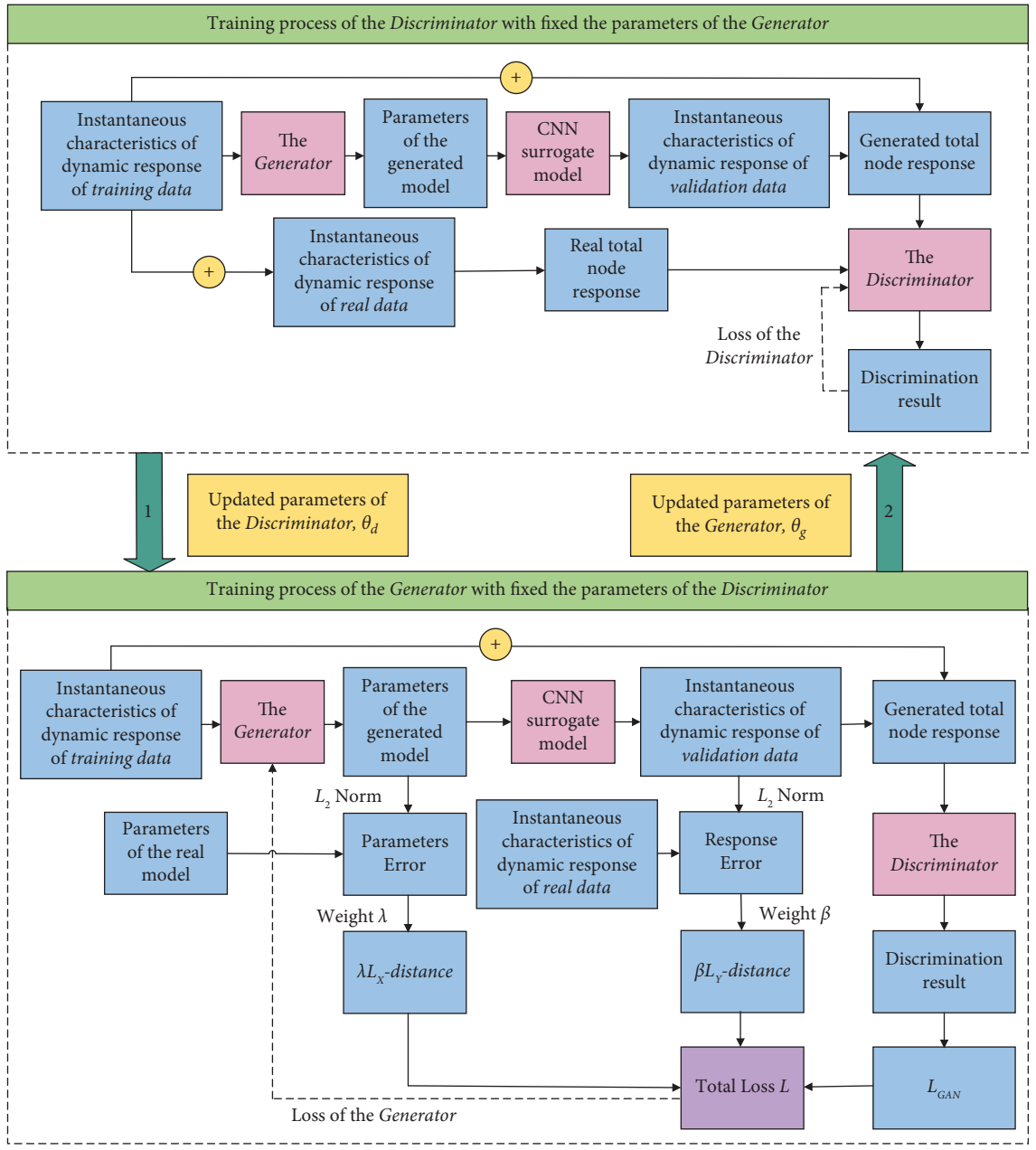

Figure 4: Adversarial training procedure of the improved GAN model.

In equation (7), it can be observed that the objective function comprises three terms. The first term is the defined loss function in the traditional GAN, and $L_{X-\text{distance}}$ and $L_{Y-\text{distance}}$ are the loss functions used to explain the misfit between real and generated samples. These terms can then be expressed using equations (8) and (9):

$$L_{X-\text{distance}} = \sum_{k=1}^{n} \frac{\left(X_k - \widehat{X}_k\right)^2}{X_k^2} \sum_{k=1}^{n} \frac{\left(X_k - \widehat{X}_k\right)^2}{X_k^2}, \tag{8}$$

$$L_{Y-\text{distance}} = \sum_{k=1}^{n} \frac{\left(Y_k - \widehat{Y}_k\right)^2}{Y_k^2}, \tag{9}$$

where n is the total number of training samples, and Y_k and $\widehat{Y}_k$ are measured and predicted structural responses, respectively. Similarly, X_k and $\widehat{X}_k$ are real and predicted nonlinear model parameters, respectively. Since the loss value calculated from L_{GAN} is considerably larger than that from $L_{X-\text{distance}}$ and $L_{Y-\text{distance}}$, two weight coefficients, λ and β, are used to balance the contributions of the three loss functions for network training. The values of these coefficients are set to 1000 in this study [42].

According to the training process described in Figure 4, the training of the improved GAN network can be achieved by performing multistep iterations, and the trained GAN network is capable of predicting nonlinear model parameters based on measured structural dynamic responses. In

numerical simulations, a steel-concrete hybrid bridge tower model subjected to seismic excitation is used to confirm the feasibility and accuracy of the improved GAN for structural nonlinear model updating. Then, shake table testing of a scaled steel–concrete hybrid bridge tower is conducted to confirm the effectiveness and reliability of the proposed method.

3. Numerical Verification

3.1. Simulated Steel-Concrete Hybrid Bridge Tower Model. The numerical simulation in this section refers to the steel-concrete hybrid bridge tower model shown in Figure 5, which was developed using the nonlinear finite element analysis software OpenSees [43]. Figure 5 shows that the bridge tower comprises two parts, the upper tower column is constructed with steel material that is connected to the lower tower column by a steel-concrete joint. The total length of the bridge tower is 2.0 m with the steel and concrete tower columns having lengths of 0.3 and 1.7 m, respectively. Detailed dimensions of the bridge tower are presented in Figure 5. For the steel-concrete hybrid bride tower, all parts are modeled using distributed plasticity beam-column elements and five Gaussian integration points are applied to these elements. The boundary conditions of the bottom tower column are assigned as fixed constraints. Figure 5 shows the sections used for the steel tower column and concrete tower column, which are simulated as fiber sections with nonlinear hysteretic materials. As shown in Figure 5, two types of fiber cross sections are designed for this structure and they are named the steel fiber section and the reinforcing concrete fiber section, respectively. The upper steel tower column is discretized into five elements with a length of 100 mm. Similarly, the low concrete tower column is discretized into 28 elements with a length of 100 mm.

The steel fibers are used to model the steel tower column by using the modified uniaxial Giuffre–Menegotto–Pinto steel model with smooth and curved-shaped loading and unloading branches, as shown in Figure 5. The material is characterized by eight parameters subdivided into three primary parameters and five secondary parameters. The three primary parameters are described as follows: elastic modulus, $E_s = 2.0 \times 10^5$ MPa, initial yield strength, $f_s = 420$ MPa, and strain hardening ratio, $b_s = 0.02$. The five secondary parameters control the curvature of hysteresis loops and isotropic hardening. The Popovics–Saenz model, which is shown in Figure 5, is employed to define the concrete behavior of the tower column, and four primary parameters are assigned: the elastic modulus $E_c = 3.5 \times 10^4$ MPa, peak compressive strength, $f_c = 23$ MPa, the strain at peak compressive strength, $\varepsilon_c = 0.002$, and the strain at the crushing strength, $\varepsilon_{cu} = 0.0033$. Moreover, the bilinear material steel01, as shown in Figure 5, in OpenSees is used to define the stress-strain relationship of the longitudinal rebars and stirrups, and three primary material parameters are set as follows: the modulus of elasticity $E_s' = 1.99 \times 10^5$ MPa, the yield strength $f_s' = 235$ MPa, and the strain hardening ratio $b_s' = 0.01$.

The Rayleigh damping is assigned for the nonlinear model and two corresponding proportional coefficients are assigned as $\alpha_0 = 1.08$ and $\alpha_1 = 0.0015$. Before performing the dynamic analysis of the hybrid tower model subjected to seismic excitation, the fundamental frequency of the structure is computed using eigenvalue analysis; the 1st natural frequency is 3.36 Hz. As shown in Figure 6, the applied base excitation of the bridge tower model is the 1994 El Centro (PGA = 0.8 g) ground acceleration record, using a time duration of 30 s. The nonlinear dynamic analysis of the steel-concrete hybrid bridge tower model is performed using the Newmark-β algorithm with a sampling rate of 50 Hz. The acceleration responses obtained from locations S_1 and S_2 of the bridge tower model are shown in Figures 7 and 8, respectively, and these acceleration responses are then used for nonlinear model updating.

3.2. Application of the Improved GAN Approach to Nonlinear Model Updating. In this study, ten parameters of the steel-concrete hybrid bridge tower model are selected as unknown parameters to be updated by the proposed nonlinear model updating approach. These parameters include the primary material parameters of the upper steel tower structure, E_s, f_s, and b_s; concrete material parameters E_c, f_c, ε_c, and ε_{cu}; and the hysteretic parameters of rebars E_s', f_s', and b_s'. The simulated structural acceleration response of the hybrid bridge tower using the theoretical values of these parameters is considered the structural response, and 5% Gaussian white noise is added to simulate acceleration responses and consider the effects of output measurement noise such as sensor and data acquisition device noise. In this study, the instantaneous amplitudes of the decomposed acceleration responses are the training data for improved GAN learning and nonlinear model updating. Because the slowly varying characteristics of the instantaneous amplitudes are comparable to the oscillation of the time series, it is not necessary to select all data points for nonlinear model updating. Thus, nonlinear model updating based on different numbers of data points is then studied in this section.

3.2.1. Effects of Data Points. In this study, the discrete analytic mode decomposition approach developed in the literature [44] is used to decompose structural acceleration responses in a finite number of mono-components. Then, the Hilbert transform is conducted to identify the instantaneous acceleration amplitudes of the decomposed structural responses. Figures 7 and 8 show that the fluctuation of the instantaneous amplitudes is obviously lower than those of the acceleration responses. Thus, nonlinear model updating with 5%, 10%, 20%, and 100% of the data points is then performed to investigate the feasibility of the proposed improved GAN approach.

According to the proposed procedure, 500 parameter combinations are stochastically generated by performing Latin hypercube sampling, and the varying range of the candidate parameters are defined as follows: $0.2\theta^{\text{true}} \le \theta \le 1.8\theta^{\text{true}}$, where θ^{true} is the theoretical value of the nonlinear model parameters. Then, these parameter

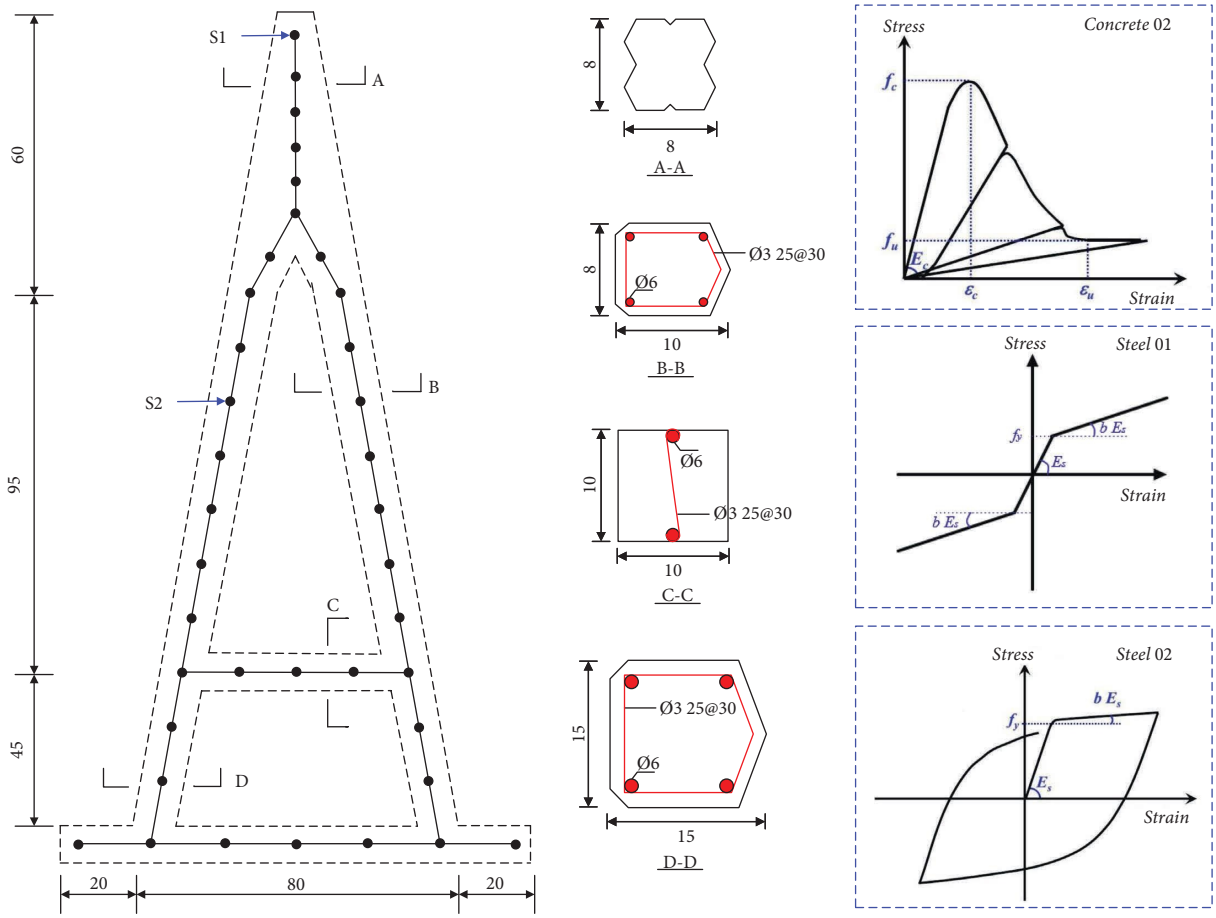

Figure 5: Steel–concrete hybrid bridge tower model simulated in OpenSees.

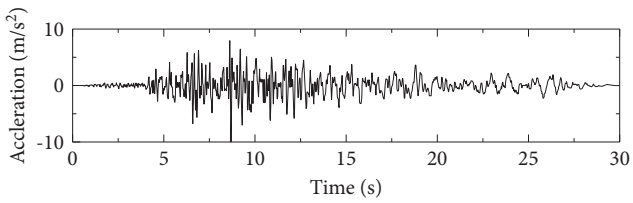

Figure 6: Applied external excitations.

combinations are substituted into the nonlinear bridge tower model to simulate structural acceleration responses under seismic excitations. The instantaneous acceleration amplitudes of the decomposed structural responses are then identified using DMAD with the Hilbert transform. The obtained testing samples are $(\theta_{\text{test}}, \mathbf{y}_{\text{test}}^{\text{amp}})$, where θ_{test} is the nonlinear parameter vector and $\mathbf{y}_{\text{test}}^{\text{amp}}$ is the identified acceleration amplitude vector under parameter samples θ_{test}. Before training the improved GAN, a CNN-based surrogate model is first trained based on training data. In the training process of the CNN model, the candidate nonlinear parameter vector is assigned as the CNN input; however, the instantaneous acceleration amplitude vector of location S_2 is set as the output. When the training of the CNN network is completed, it can be then integrated into the GAN for the nonlinear model updating. To ensure the trained improved GAN is capable of accurately constructing the mapping relationship between the nonlinear parameters and instantaneous acceleration amplitudes, the identified instantaneous acceleration amplitudes of the structural responses obtained at location S_1 are used as training data and the corresponding instantaneous acceleration amplitudes at location S_2 are used as validation data.

In this numerical simulation, the convergence process for the training of the CNN-based surrogate model under four cases is shown in Figure 9. The training loss and validation loss are obviously decreased during the first 50 epochs, and the loss values gradually tend to be stationary after running 50 epochs; however, it should be pointed out that the convergence processes are not smooth convergences. During training, network parameters with the smallest validation loss are maintained for testing, which contributes to the optimal performance of the network, and the best points at the smallest validation loss are labeled with green stars in Figures 9(a)–9(d). As shown in Figure 9, the validation loss values are smaller than those of training loss, which indicates that no overfitting occurs during the training process. Thus, the CNN with optimized network parameters, presented in Figure 9, is used as the surrogate model of the improved GAN. When the construction of the improved GAN is achieved, 500 testing samples are used for the training of the discriminator according to the proposed network training process. During the training process, the

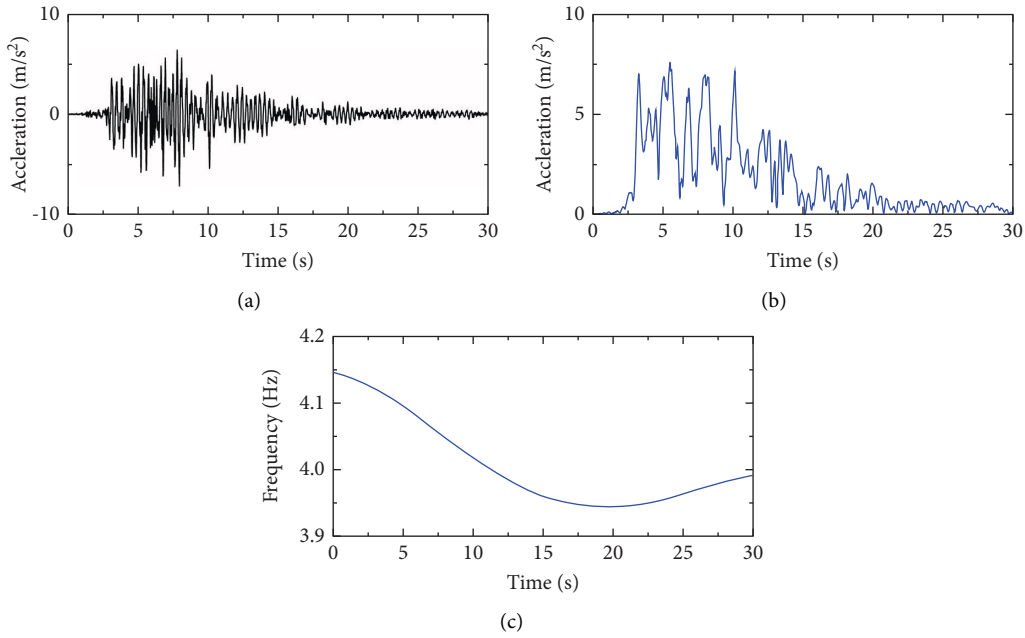

FIGURE 7: Characteristics of the hybrid bridge tower model at location S_1: (a) acceleration response; (b) instantaneous acceleration amplitude; (c) instantaneous frequency.

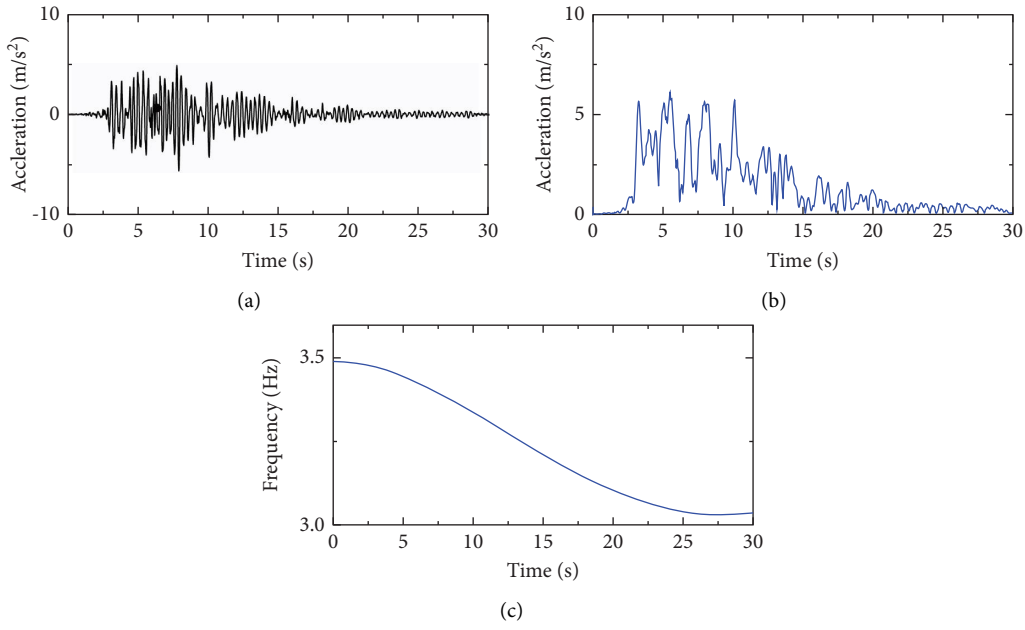

FIGURE 8: Characteristics of the hybrid bridge tower model at location S_2: (a) acceleration response; (b) instantaneous acceleration amplitude; (c) instantaneous frequency.

instantaneous acceleration amplitudes obtained from structural responses at location S_1 are considered as the input of the generator, while the data from location S_2 is set as the validation samples. The number of training epochs and the learning efficiency parameter of the improved GAN are set to 300 and 4×10^{-4}, respectively. Furthermore, the dropout technique is applied in this study and 50% of the neurons are dropped during the training process; this indicates that only half of the network parameters are trained in each epoch to enhance the generalization capability of the generator model. Figure 10 shows the training process of the improved GAN in four cases. The training loss and validation loss of the four cases are significantly reduced during the first 50 epochs, and the loss values of these loss curves converge to smaller values after 100 epochs. Note that the validation loss values of the four cases are smaller than the training loss values, which suggests that no overfitting occurs during the training process. The best points at the smallest validation loss of the network training are

labeled with green stars in Figures 10(a)–10(d). As shown in Figure 10(a), when 5% of the data points are selected as training samples, the validation loss of the improved GAN reaches to the smallest loss of 6% at the 295th training iteration. In Case 2, as shown in Figure 10(b), the best network model is obtained at the 287th training with the smallest loss of 5.75%. Similarly, as shown in Figure 10(c), the GAN in case 3 achieves the smallest loss of 4.43% after running 260 steps. As shown in Figure 10(d), the smallest value of 5.26% is achieved at the 296th iteration when 100% of the data points are used for network training. After the training of the improved GAN is achieved, the improved GAN model with the smallest validation loss value is retained as the optimized network model for nonlinear model updating.

In this study, the simulated acceleration responses with 5% Gaussian white noise are assumed as the measured dynamic responses of the steel-concrete hybrid bridge tower model, and the instantaneous amplitudes of the measured structural responses can be identified using the discrete analytic mode decomposition with the Hilbert transform method. Then, using 5%, 10%, 20%, and 100% of the data points of the identified instantaneous acceleration amplitudes as the input of the trained and improved GAN model, the estimated nonlinear model parameters under the four cases are presented in Table 2. Furthermore, by substituting the identified nonlinear model parameters into the initial nonlinear model, the predicted structural response at location S_1 under Case 1 is displayed in Figure 11. As observed from Table 2 and Figure 11, the nonlinear model parameters can be accurately estimated based on the trained and improved GAN model and the predicted acceleration responses match with the measured structural dynamic responses. To reliably evaluate the accuracy of the model updating results, three error indices, R_{acc}, R_{amp} and R_{ω}, are defined as follows:

$$R_{\text{acc}} = \frac{\left\| A_{\text{acc}}^{\text{predict}}(t) - A_{\text{acc}}(t) \right\|_2}{\left\| A_{\text{acc}}(t) \right\|_2} \times 100\%, \tag{10}$$

$$R_{\text{amp}} = \frac{\left\| A_{\text{amp}}^{\text{predict}}(t) - A_{\text{amp}}(t) \right\|_2}{\left\| A_{\text{amp}}(t) \right\|_2} \times 100\%, \tag{11}$$

$$R_{\omega} = \frac{\left\| \omega^{\text{predict}}(t) - \omega(t) \right\|_2}{\left\| \omega(t) \right\|_2} \times 100\%, \tag{12}$$

where $A_{\text{acc}}^{\text{predict}}(t)$ and $A_{\text{acc}}(t)$ are the acceleration responses from the analytical and testing models, respectively; $A_{\text{amp}}^{\text{predict}}(t)$ and $A_{\text{amp}}(t)$ are the instantaneous acceleration amplitudes of the analytical and testing models, respectively; $\omega^{\text{predict}}(t)$ and $\omega(t)$ are the slowly-varying parts of the instantaneous frequencies obtained from the analytical and testing models, respectively; and $\| \cdots \|_2$ is the L_2 norm. Based on previous studies of the authors [22], the instantaneous amplitude and frequency are two significant indices used to describe the characteristics of a nonstationary signal; thus, in this study, the accuracy of the model updating results is evaluated by comparing the acceleration responses and the instantaneous amplitudes and frequencies from the calibrated nonlinear model and the testing structure. Based on the acceleration responses and the instantaneous amplitudes and frequencies of the estimated and measured structural dynamic responses, the calculated error indices are shown in Table 3. As shown in Table 3, the three error indices for the four cases are less than 3% when more than 5% of the data points are selected.

To validate that the proposed approach can significantly save computational cost, the computational time for each case, using a Tsinghua Tongfang desktop workstation with an Intel(R) Core(TM) i7-10700 CPU @ 2.90 GHz 16.0 GB RAM is listed in Table 3. As can be seen from Table 3, the required computational time significantly decreases when fewer data points are used for nonlinear model updating. The primary reason for this could be that using a smaller number of data points will significantly decrease the complexity of nonlinear parameter estimation when using the proposed method. Therefore, the abovementioned analysis results indicate that the proposed improved GAN model trained with 5% of the data points is reliable and accurate for nonlinear model updating, and computation efficiency is obviously improved compared with Case 4.

3.2.2. Effects of Measurement Noise. To examine the noise effect, simulated accelerations with 10% and 20% white noise are used for identification analysis. In this section, the same ten nonlinear parameters, E_s, f_s, b_s, E_c, f_c, ε_c, ε_{cu}, E_s', f_s', and b_s' were selected. According to the analysis results in Section 3.2.1, 5% of the data points selected from the instantaneous amplitudes of the decomposed structural acceleration responses are used as training data for the improved GAN model. Based on the proposed nonlinear model updating procedure, the improved GAN is first trained using the generated data samples based on the nonlinear model, and then the trained improved GAN model is applied for identifying nonlinear model parameters. Tables 4 and 5 are the updated nonlinear parameters and the calculated error indices. Table 4 shows that the proposed improved GAN model can accurately identify nonlinear model parameters using the measured instantaneous acceleration amplitudes as the input. As shown in Table 5, the calculated error indices are less than 12%, even under the effect of 20% measurement noise, which indicates that the proposed improved GAN approach can achieve structural nonlinear model updating with better noise robustness.

3.2.3. Comparison of the Identification Results between the CNN and Improved GAN. Compared with the conventional methods and mechanical models for nonlinear model updating, the improved GAN takes the instantaneous acceleration amplitude and instantaneous frequency with a slow varying portion of the principal component response as nonlinear indices to quantify the nonlinear response with time-varying characteristics. Meanwhile, on the basis of the traditional GAN, the pooling layer in the CNN is replaced by the convolution layer, and the mapping relationship between the nonlinear model parameters and the instantaneous characteristic response is subsequently established by the

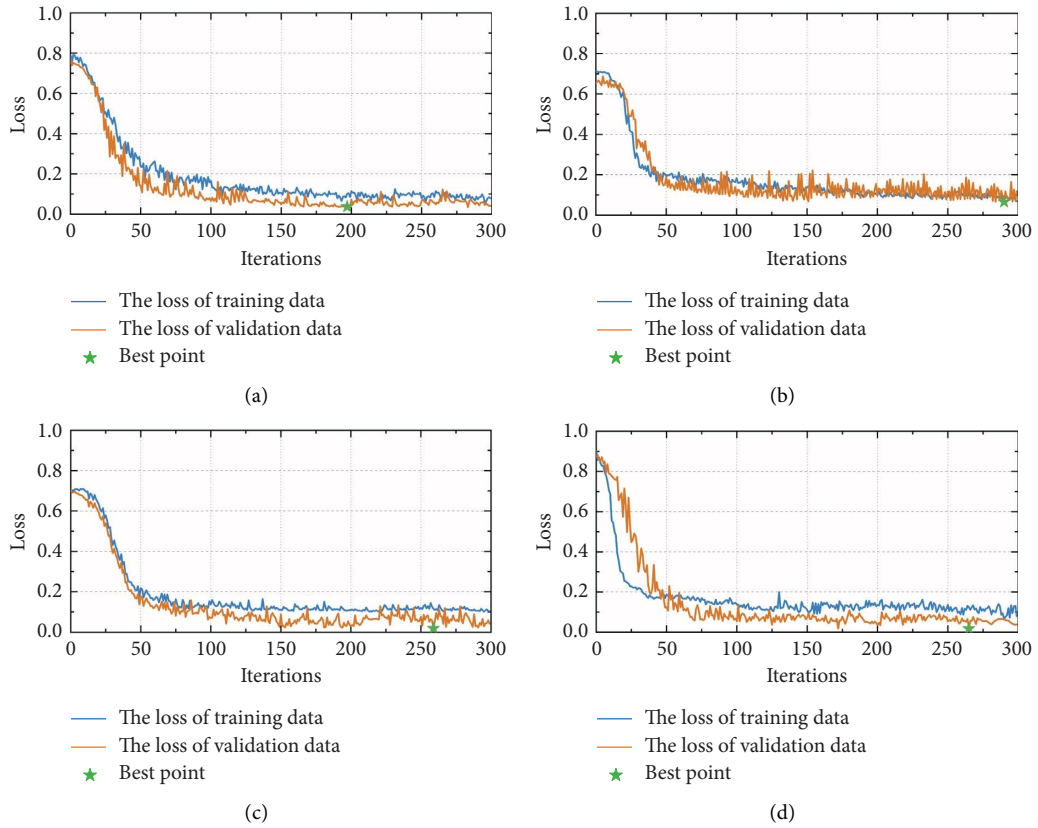

Figure 9: Training process of the CNN-based surrogate model with: (a) 5%; (b) 10%; (c) 20%; (d) 100% of the data points.

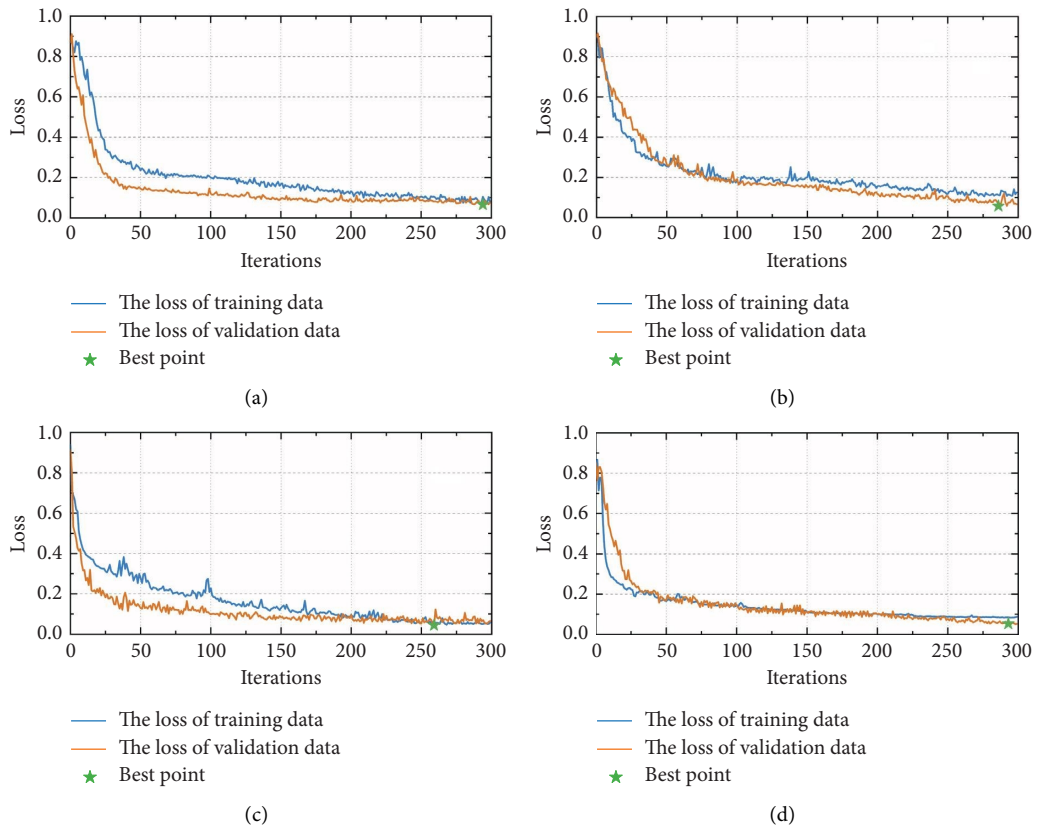

Figure 10: Training process of the improved GAN with: (a) 5%; (b) 10%; (c) 20%; (d) 100% of the data points.

Table 2: Parameter estimate results for four different data point cases.

Data points	Model parameters									
	Steel 01			*Concrete 02*					*Steel 02*	
	E_s/E_s^{real}	f_s/f_s^{real}	b_s/b_s^{real}	E_c/E_c^{real}	f_c/f_c^{real}	$\varepsilon_c/\varepsilon_c^{real}$	$\varepsilon_{cu}/\varepsilon_{cu}^{real}$	$E_s'/(E_s')^{real}$	$f_s'/(f_s')^{real}$	$b_s'/(b_s')^{real}$
Case 1 (5%)	0.97	1.03	1.05	0.98	1.05	0.98	0.96	0.98	1.02	0.98
Case 2 (10%)	0.98	0.98	0.97	1.02	1.04	0.98	1.01	0.98	1.02	0.99
Case 3 (20%)	1.02	0.99	0.99	1.01	0.98	1.02	1.00	1.01	0.99	1.00
Case 4 (100%)	1.01	1.00	0.99	0.99	1.01	0.99	1.00	0.99	1.00	1.00

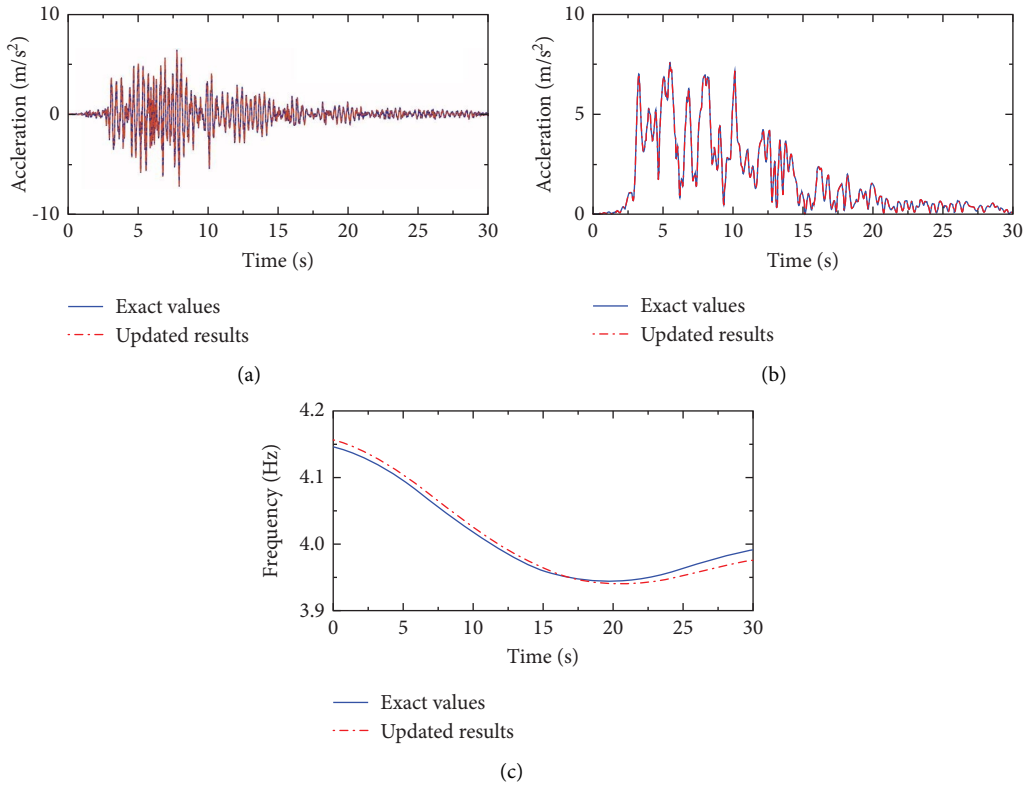

Figure 11: Comparison of calibrated results with the true structural response under Case 1: (a) acceleration response; (b) instantaneous acceleration amplitude; (c) instantaneous frequency.

Table 3: Error indices and computational time for four different data point cases.

Data points	Case 1 (5%)	Case 2 (10%)	Case 3 (20%)	Case 4 (100%)
R_{acc} (%)	7.39	2.07	0.89	0.88
R_{amp} (%)	4.28	1.65	0.57	0.52
R_ω (%)	1.38	0.07	0.05	0.02
Computational time (min)	3.6	12.3	31.4	175.1

Table 4: Parameter estimate results for two different noise levels.

Noise levels	Model parameters									
	Steel 01			*Concrete 02*					*Steel 02*	
	E_s/E_s^{real}	f_s/f_s^{real}	b_s/b_s^{real}	E_c/E_c^{real}	f_c/f_c^{real}	$\varepsilon_c/\varepsilon_c^{real}$	$\varepsilon_{cu}/\varepsilon_{cu}^{real}$	$E_s'/(E_s')^{real}$	$f_s'/(f_s')^{real}$	$b_s'/(b_s')^{real}$
Case 1 (10%)	0.97	0.97	0.96	1.03	1.06	1.04	0.94	0.98	0.98	0.96
Case 2 (20%)	1.04	0.94	0.94	1.06	1.07	0.95	0.93	1.04	0.96	0.94

Table 5: Error indices of parameter estimate results for two different noise levels.

Noise levels	Case 1 (10%)	Case 2 (20%)
R_{acc} (%)	9.21	11.77
R_{amp} (%)	5.50	6.74
R_{ω} (%)	1.36	2.56

CNN surrogate model to enhance the fitting ability of the network. In this section, to highlight the advantages of using the improved GAN for structural nonlinear model updating, the identified results of the improved GAN are compared with those obtained using CNN. In nonlinear model updating, the same DenseNet, which aims to avoid the negative effects of the network layer structures, is used for the CNN and the improved GAN. During the CNN and improved GAN training process, 5% of the data points selected from the instantaneous amplitudes of structural acceleration responses are defined as the network input, and a total of 500 sets of training samples are used for network training. The same computational device described in Section 3.2.1 is applied for network training, and the identification results of nonlinear parameters are presented in Table 6. The corresponding calculated error indices and computational times of the two networks are illustrated in Table 7. Table 7 shows that the two types of networks are capable of accurately achieving structural nonlinear parameter identification. However, as shown in Tables 6 and 7, although the required computational time of the CNN is slightly less than that of the improved GAN, the estimated accuracy of the trained improved GAN is higher than that of the CNN. The abovementioned results confirm that the proposed improved GAN is accurate and reliable for structural nonlinear model updating.

4. Experimental Application

4.1. Shake Table Test of a Scaled Steel-Concrete Hybrid Bridge Tower Structure. To validate the effectiveness of the proposed method for structural nonlinear model updating, a scaled steel-concrete hybrid bridge tower, as shown in Figures 12 and 13, was constructed in the Structural Dynamics Lab at Hefei University of Technology. The tested structure was developed by referring to a real steel-concrete hybrid bridge tower with a scale of 1 : 172. The full length of the scaled bridge tower structure is 2.0 m, and the bridge tower comprises two parts: the upper steel tower column and a lower tower column. Figure 12 shows that these two parts of the bridge tower are 0.6 and 1.45 m, respectively. Based on the design files, the upper tower column is designed as a stel structure with a yield strength of 420 MPa. The lower tower was constructed as a reinforced concrete structure, and the concrete material applied for these parts was set as C60 based on the Chinese codes for the design of concrete structures. The measured ultimate strength of the longitudinal rebars and stirrups used for the concrete tower was 616 and 430 MPa, respectively. In this study, the steel-concrete joint of the tested structure was simplified to be a fixed connection because of the significant complexity of construction of the joint in the original steel–concrete bridge tower structure. Figure 14 shows the detailed geometric dimensions and the rebar arrangement of the concrete sections. To ensure the stability of the bridge tower model during structural vibration, the concrete bearing platform shown in Figure 12(a) was designed at the bottom of the bridge tower structure. The geometric size of this concrete block was 1.20 m × 1.20 m × 0.1 m. Furthermore, to ensure the scaled bridge tower structure has the approximate physical characteristics of the actual structure, it was necessary to add additional mass to the tested structure. According to the counterweight design, 61 mass blocks were applied to the bridge tower structure and the detailed information on the added mass can be found in Figure 12(b). Three different types of mass blocks were applied to the tested structure and they are referred to as mass blocks *A*, *B*, and *C*. The weights of mass blocks *A*, *B*, and *C* were 4.0, 6.28, and 94.0 kg, respectively. The total mass of the scaled steel–concrete hybrid bridge tower is 1068 kg, including the tower column at 306 kg, the concrete platform of 313 kg, and the additional mass of 450 kg.

During the shake table testing, six single-direction accelerometers, shown in Figure 13, were installed on the tested structure to obtain horizontal acceleration responses under seismic excitation. These accelerometers are referred to as Acc-1, Acc-2, ..., Acc-6. An additional sensor, B_1, was installed on the shake table to record the base excitation of the tested structure. A National Instruments data acquisition system was used to record structural dynamic responses with a sampling rate of 200 Hz. Because the primary purpose of this shake table testing was to examine the damage process of the bridge tower structure subjected to seismic excitation, different types of seismic excitations were selected as the input of the bridge tower structure with a maximum peak ground acceleration varying from 0.1 g (g denotes gravity acceleration) up to the collapse of the structure having an interval of 0.1 g; the tested structure was then destroyed when the amplitude of the applied external excitations reached 0.8 g. In this study, for nonlinear model updating, the measured dynamic responses of the bridge tower structure subjected to a high-amplitude seismic wave were applied and the applied external excitation was regenerated ground motion recorded at the Oxnard Boulevard station during the 1994 Northridge earthquake (PGA = 0.7 g), as shown in Figure 15. Before testing, a low-amplitude Gaussian white noise time series was selected as the input of the bridge tower structure, and then the obtained dynamic responses were used to identify structural modal information such as natural frequencies and mode shapes.

4.2. Nonlinear Model Updating Based on the Proposed GAN Approach. Based on the detailed geometric and material parameters of the scaled steel–concrete hybrid bridge tower, the nonlinear bridge tower model was modeled using OpenSees. The nonlinear bridge tower model is discretized into 18 lump masses connected to each other with beam-column fiber section elements, and the cross-sectional

Table 6: Parameter estimate results were obtained using two different approaches.

Different models	Model parameters									
	Steel 01			*Concrete 02*				*Steel 02*		
	E_s/E_s^{real}	f_s/f_s^{real}	b_s/b_s^{real}	E_c/E_c^{real}	f_c/f_c^{real}	$\varepsilon_c/\varepsilon_c^{\text{real}}$	$\varepsilon_{cu}/\varepsilon_{cu}^{\text{real}}$	$E_s'/(E_s')^{\text{real}}$	$f_s'/(f_s')^{\text{real}}$	$b_s'/(b_s')^{\text{real}}$
Case 1 (GAN)	0.97	1.03	1.05	0.98	1.05	0.98	0.96	0.98	1.02	0.98
Case 2 (CNN)	1.04	0.95	0.90	1.03	1.05	0.95	0.92	0.96	0.97	0.95

Table 7: Error indices and computational time for two different approaches.

Different models	Case 1 (GAN)	Case 2 (CNN)
R_{acc} (%)	7.39	12.17
R_{amp} (%)	4.28	7.00
R_{ω} (%)	1.38	1.41
Computational time (min)	3.6	3.3

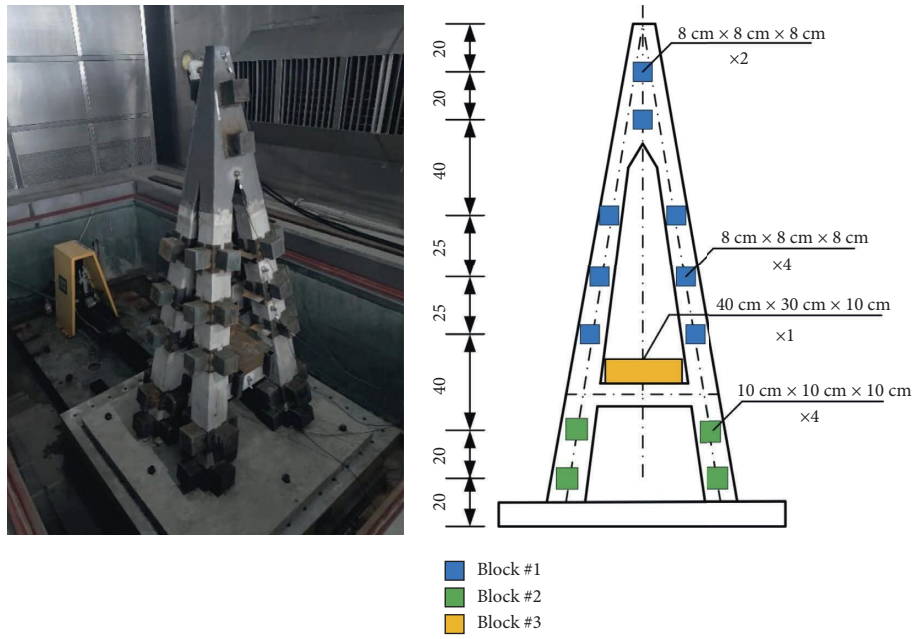

Figure 12: The test specimen: (a) scaled bridge tower structure; (b) counterweight design of the bridge tower structure.

dimensions are simulated according to the tested structure. In this nonlinear model, all tower columns, including the upper steel tower columns and the lower tower columns, are assigned as nonlinear force-basedbeam-column elements. Moreover, the linear elastic beam-column elements are applied to define the links between the upper steel tower and the lower tower column. Three different types of nonlinear material models are used to define the nonlinear characteristics of the bridge tower model under seismic excitation. The modified uniaxial Giuffre–Menegotto–Pinto steel model is used to define the stress-strain relations of the steel material in the upper tower column, and *Concrete 02,* and *Steel 02* available in OpensSees and are shown in Figure 5 in Section 3.1 are employed to represent the uniaxial constitutive laws of the concrete and reinforcing steel, respectively. Based on the parameter sensitivity analysis results described by the numerical simulation, ten material parameters are selected as the candidate parameters for nonlinear model updating. Once the nonlinear model is developed, the proposed GAN approach can then be applied to calibrate the nonlinear parameters by minimizing the response errors between the nonlinear model and the tested structure. According to the proposed nonlinear model updating procedure, 500 parameter combinations are stochastically generated by performing the Latin hypercube sampling and the varying range of the candidate parameters are defined as follows: $0.2\theta^{\text{initial}} \le \theta \le 1.8\theta^{\text{initial}}$. Then, these parameter combinations are substituted in the initial nonlinear model to simulate structural acceleration responses under seismic excitations.

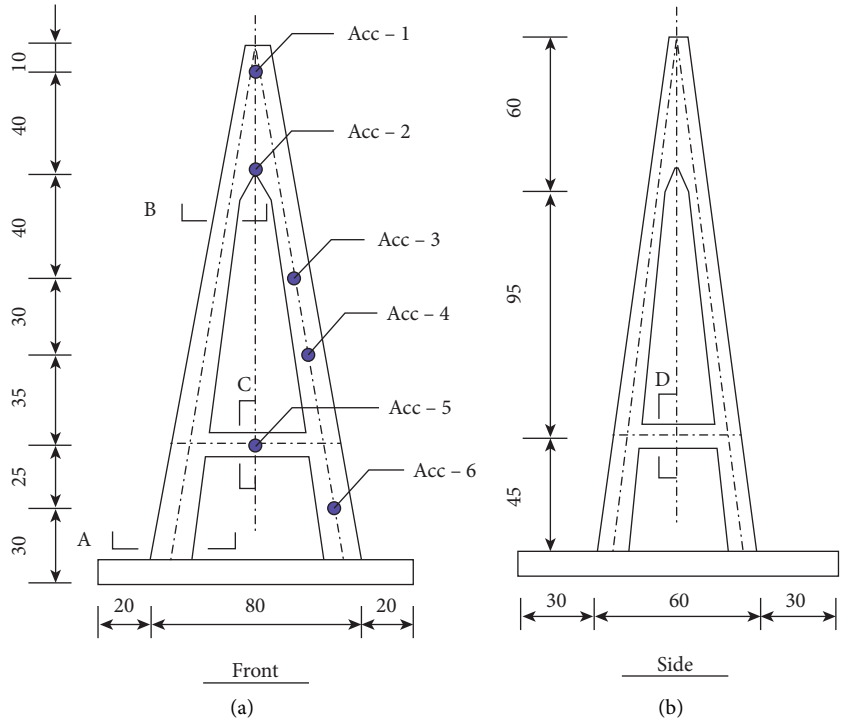

FIGURE 13: Geometric dimensions of the scaled bridge tower model (in cm): (a) front; (b) side.

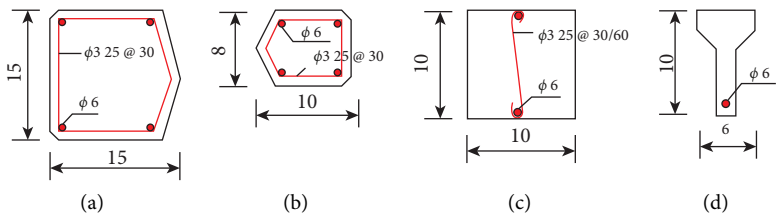

FIGURE 14: Detailed geometric dimensions and rebar arrangement of the concrete sections (in cm): (a) A-A; (b) B-B; (c) C-C; and (d) D-D sections.

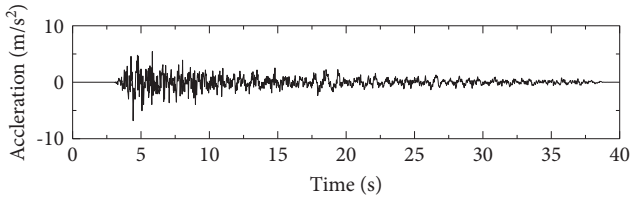

FIGURE 15: Applied external excitations.

After performing dynamic analysis, the primary mono-components of the simulated structural dynamic responses can be identified using the improved GAN approach. Then, 5% of the data points selected from the identified mono-components can then be employed as the training data for the surrogate model and improved GAN network; the training process is shown in Figure 16. Note from Figure 16 that the training and validation losses of the improved GAN model were significantly reduced in the first several iterations. Similarly, Figure 16 shows that the CNN reaches the smallest validation loss of 7.14% at the 82nd iteration and the GAN reaches the smallest validation loss of 10.79% at the 48th iteration. The training results indicate that the trained and improved GAN network has strong generalization ability, which would be effectively applied for a nonlinear model updating based on structural dynamic responses. The trained and improved GAN can then be employed to calibrate the nonlinear model of the tower structure using the measured structural dynamic responses. In this study, the first two mono-components of the measured acceleration responses from sensors Acc-1 to Acc-5 are first identified, and 5% of the data points selected from these components are considered as input to the generator of the trained improved GAN. The best optimized nonlinear parameters can be identified based on the trained and improved GAN and the updated nonlinear material parameters are listed in Table 8. Table 8 shows that the changes in the candidate nonlinear parameters are obvious when compared with the initial values, which indicates that these selected nonlinear parameters are sensitive to structural dynamic responses.

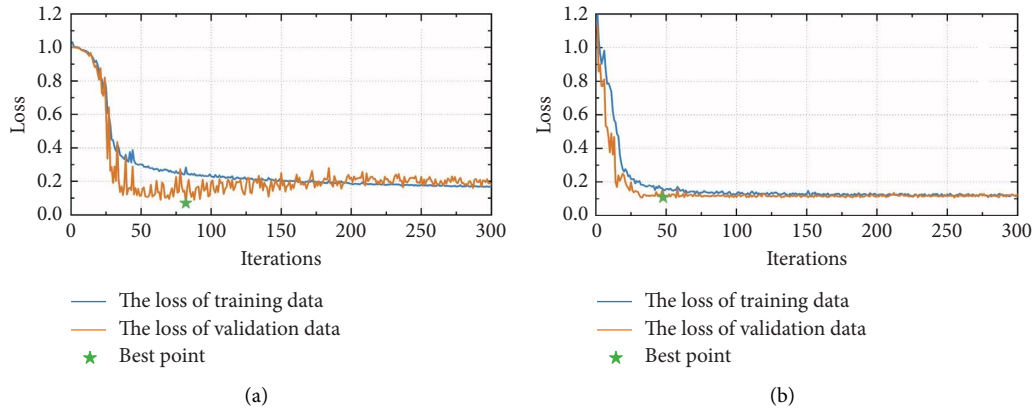

Figure 16: Training process of the improved GAN for the (a) CNN-based surrogate model; (b) the improved GAN.

Table 8: Updated results of the steel–concrete hybrid bridge tower model.

Parameters	*Steel 01*			*Concrete 02*				*Steel 02*		
	E_s (GPa)	f_s (MPa)	b_s	E_c (GPa)	f_c (MPa)	ε_c ($\times 10^{-3}$)	ε_{cu} ($\times 10^{-3}$)	E_s' (GPa)	f_s' (MPa)	b_s'
Initial values	210	235	0.01	36	38.5	2	3.3	210	420	0.02
Updated values	232	242	0.016	36.2	37.2	1.7	2.9	225	408	0.017

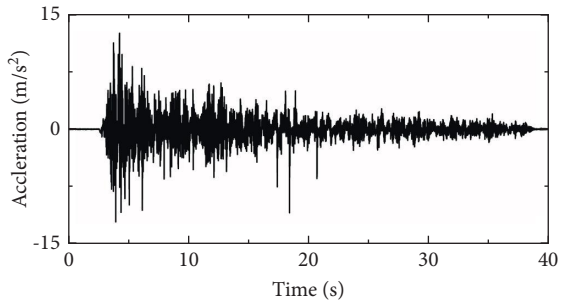

Figure 17: Acceleration response of the bridge tower structure at the top.

When the nonlinear parameters are identified based on the improved GAN approach, they can substitute the updated hysteretic material parameters in the nonlinear model to predict structural dynamic responses. By performing nonlinear dynamic responses, the simulated structural acceleration responses and instantaneous characteristics based on the calibrated nonlinear model are shown in Figures 17–19. A comparison of the acceleration responses and identified instantaneous characteristics between the updated nonlinear model and tested structure is illustrated in Figures 20–22. Figures 20–22 show that the calibrated nonlinear model is capable of predicting the nonlinear dynamic characteristics of the steel–concrete hybrid bridge tower structure under strong seismic excitations with better accuracy. Moreover, to quantify the prediction accuracy of the updated nonlinear model, the defined error index in equations (10) to (12) is employed to calculate the predicted error of acceleration responses; the identified instantaneous amplitudes are presented in Table 9. The calculated error indices of these instantaneous parameters are obviously larger than those in the numerical simulation. This is because significant modeling errors will occur when using a simplified nonlinear model to characterize the complex dynamic behaviors of the testing structure. However, because the error indices are calculated based on comparing the instantaneous amplitudes of the whole time history, which reflect the global error of structural responses, the calculated error index results are usually large. Even a small difference in time domain responses would lead to a relatively high error indices value. Therefore, the above-mentioned experimental results suggest that the proposed improved GAN approach is capable of structural nonlinear model updating.

4.3. Nonlinear Model Evaluation. An appropriately updated nonlinear model shall be able to accurately predict the dynamic responses of structures subjected to known or unknown external excitations. Verifying the mismatch of the

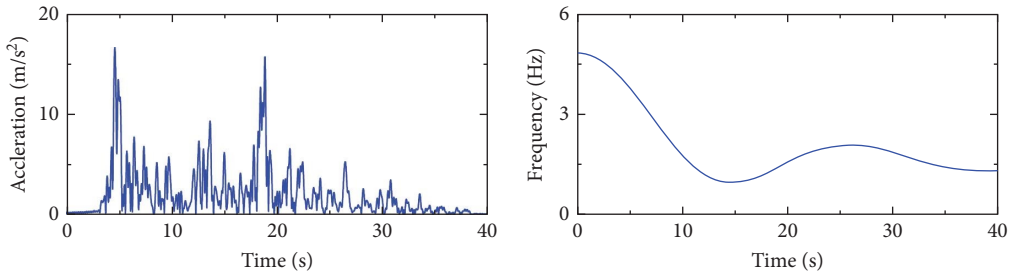

FIGURE 18: Instantaneous characteristics of the first mono-component response of the bridge tower structure at the top: (a) instantaneous acceleration amplitude; (b) instantaneous frequency.

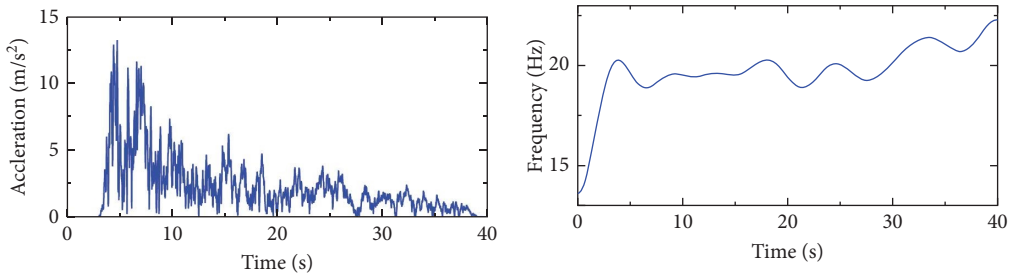

FIGURE 19: Instantaneous characteristics of the second mono-component response of the bridge tower structure at the top: (a) instantaneous acceleration amplitude; (b) instantaneous frequency.

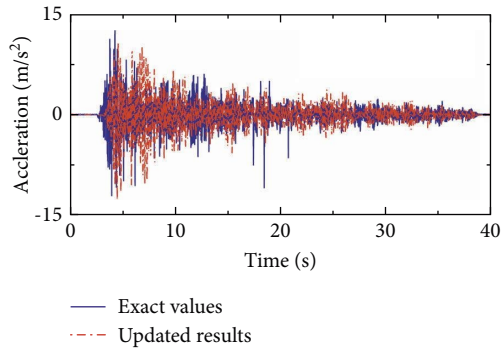

FIGURE 20: Comparison between the acceleration response of the bridge tower structure at the top obtained by the updated nonlinear model and the tested structure.

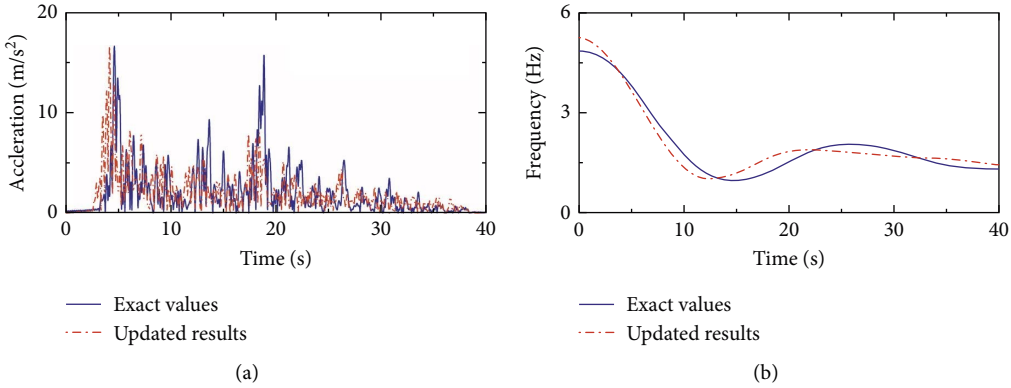

FIGURE 21: Comparison between the first mono-component obtained by the updated nonlinear model and the tested structure: (a) instantaneous acceleration amplitude; (b) instantaneous frequency.

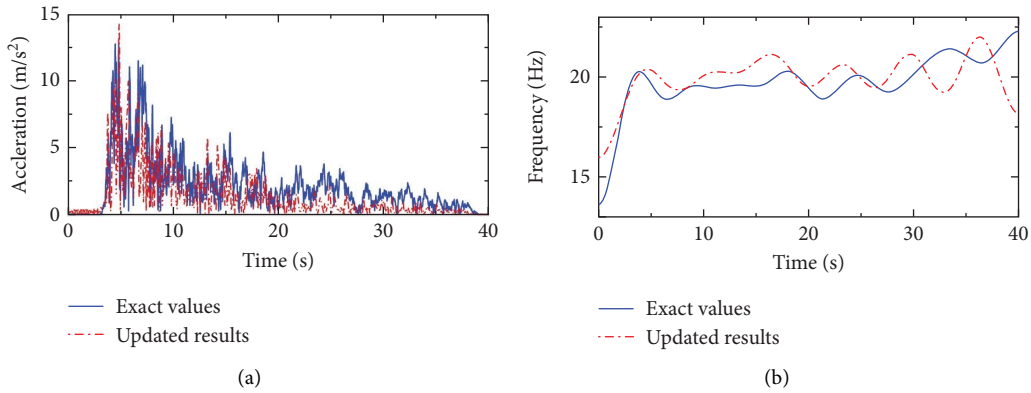

Figure 22: Comparison between the second mono-component obtained by the updated nonlinear model and the tested structure: (a) instantaneous acceleration amplitude; (b) instantaneous frequency.

Table 9: Error indices based on updated and measured results.

R_{acc} (%)	R_{amp}^{1st} (%)	R_{ω}^{1st} (%)	R_{amp}^{2nd} (%)	R_{ω}^{2nd} (%)
14.6	5.6	1.2	7.3	6.8

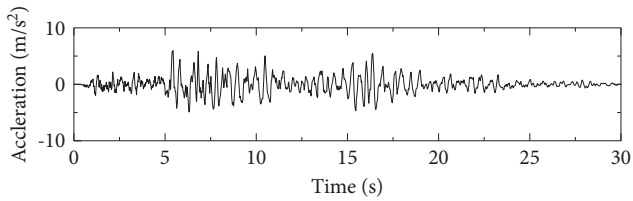

Figure 23: Applied external excitation for nonlinear model evaluation.

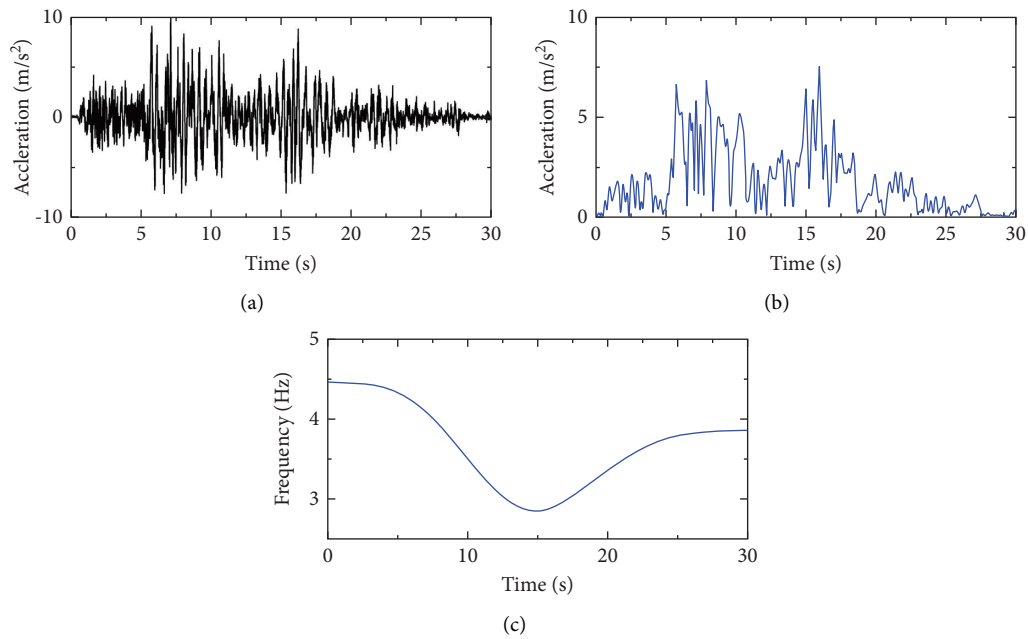

Figure 24: Instantaneous characteristics of the first mono-component response: (a) acceleration response; (b) instantaneous acceleration amplitude; (c) instantaneous frequency.

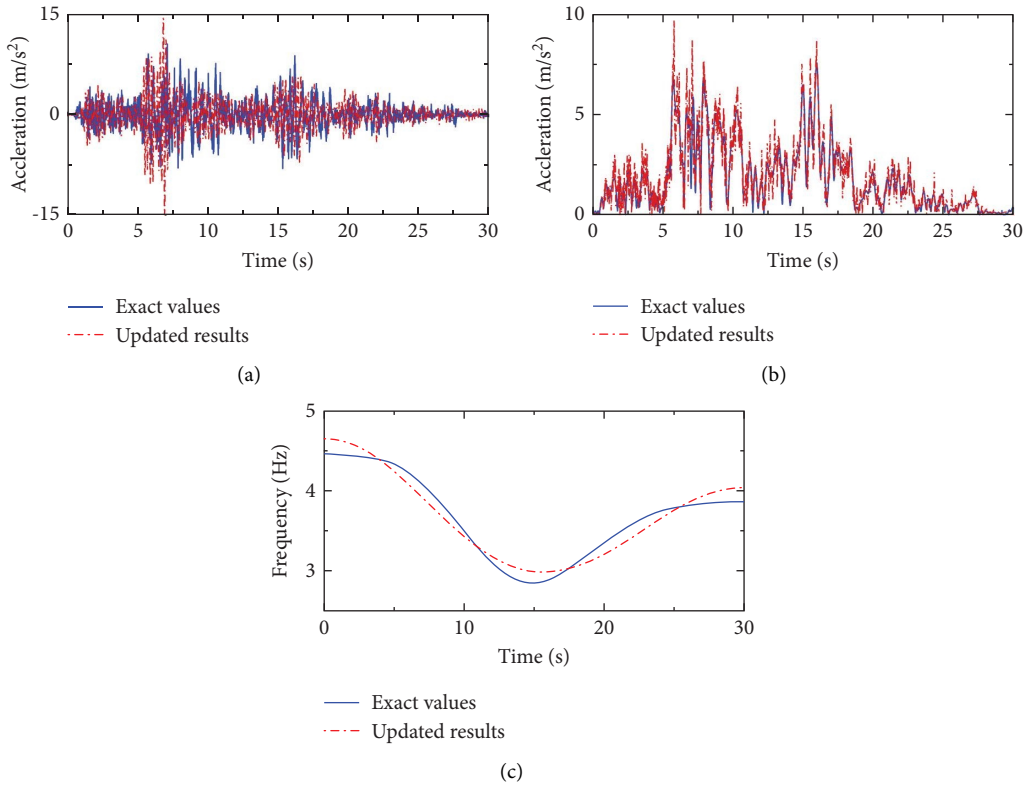

Figure 25: Comparison of calibrated results with the true structural responses: (a) acceleration response; (b) instantaneous acceleration amplitude; (c) instantaneous frequency.

Table 10: Calculated error indices under a new external excitation.

R_{acc} (%)	R_{amp}^{1st} (%)	R_{ω}^{1st} (%)
13.7	2.5	1.7

dynamic response between the updated nonlinear model and the tested structures under a new seismic excitation is an important approach to evaluate the reliability of the calibrated nonlinear model. Hence, to validate the effectiveness of the updated steel–concrete hybrid bridge tower model, a new strong seismic excitation, shown in Figure 23, is applied as a base excitation of the nonlinear model. By performing nonlinear dynamic analysis, the estimated structural instantaneous characteristics at the top of the bridge tower model are presented in Figure 24. A comparison of the identified instantaneous parameters of the decomposed acceleration responses between the nonlinear model and the tested structure is illustrated in Figure 25. The calculated error indices of the acceleration responses and the instantaneous amplitudes and frequencies of the decomposed first mono-component are listed in Table 10. Figures 24 and 25 show that the updated nonlinear model can effectively predict structural nonlinear dynamic responses subjected to the new external excitations. Moreover, by comparing the calculated error indices with Section 4.2, note that the values of the calculated error indices do not considerably increase, even under the new seismic excitations. Based on the analysis results, the proposed improved GAN approach is reliable and accurate for nonlinear model updating and the predicted responses are in acceptable error.

5. Conclusions

In this study, an improved GAN based on the instantaneous characteristics of decomposed structural dynamic responses is proposed for the nonlinear model updating of a bridge tower subjected to seismic excitation. According to the proposed approach, a CNN surrogate model is used to enhance the learning capability of the discriminator network, and the instantaneous characteristics of the decomposed structural acceleration responses are employed as training samples of the improved network model. Then, the trained GAN model can be applied to identify optimal nonlinear model parameters based on the measured instantaneous acceleration amplitude of structures. The proposed method is then verified by simulating a nonlinear tower model and shake table testing on a scaled steel–concrete hybrid bridge tower structure. Based on the numerical and experimental results, the following conclusions can be obtained:

(1) The application of the CNN-based surrogate model can enhance the capability of the discriminator network to learn the complex mapping relationship

between structural vibration responses and nonlinear model parameters.

(2) The trained GAN model can effectively identify optimal nonlinear model parameters using the measured instantaneous acceleration amplitudes of the structural responses. The identified results indicate that the proposed method has better noise robustness.

(3) By comparing the nonlinear model updating results between the improved GAN and a CNN, the proposed network model is suggested as more suitable for structural nonlinear model updating in this study.

(4) The feasibility and reliability of the proposed nonlinear model updating approach have been successfully validated by numerical simulations and shake table tests on a steel-concrete hybrid bridge tower subjected to seismic excitation.

Data Availability

The data used to support the findings of this study will be available from the corresponding author upon reasonable request.

Conflicts of Interest

The authors declare that they have no conflicts of interest.

Acknowledgments

Financial support to complete this study was provided in part by the National Natural Science Foundation of China under grant nos. 51922036 and 52278301, by the Fundamental Research Funds for the Central Universities under grant nos. JZ2020HGPB0117 and JZ2022HGTA0334, and by the Science Technology Research and Development Program Project of China Railway Group Co., Ltd. (2020-major-01). The results and opinions expressed in this paper are those of the authors only and they do not necessarily represent those of the sponsors.

References

[1] M. I. Friswell and J. E. Mottershead, *Finite Element Model Updating in Structural Dynamics*, p. 304, Kluwer Academic Publishers, The Netherlands, 1995.

[2] C. P. Fritzen, D. Jennewein, and T. Kiefer, "Damage detection based on model updating methods," *Mechanical Systems and Signal Processing*, vol. 12, no. 1, pp. 163–186, 1998.

[3] J. M. W. Brownjohn, P. Q. Xia, H. Hao, and Y. Xia, "Civil structure condition assessment by FE model updating," *Finite Elements in Analysis and Design*, vol. 37, no. 10, pp. 761–775, 2001.

[4] D. S. Shan, Q. Li, I. Khan, and X. H. Zhou, "A novel finite element model updating method based on substructure and response surface model," *Engineering Structures*, vol. 103, pp. 147–156, 2015.

[5] B. Moaveni and I. Behmanesh, "Effects of changing ambient temperature on finite element model updating of the Dowling Hall Footbridge," *Engineering Structures*, vol. 43, pp. 58–68, 2012.

[6] B. Hofmeister, M. Bruns, and R. Rolfes, "Finite element model updating using deterministic optimisation: a global pattern search approach," *Engineering Structures*, vol. 195, pp. 373–381, 2019.

[7] B. Jaishi and W. X. Ren, "Structural finite element model updating using ambient vibration test results," *Journal of Structural Engineering*, vol. 131, no. 4, pp. 617–628, 2005.

[8] W. X. Ren, S. E. Fang, and M. Y. Deng, "Response surface–based finite-element-model updating using structural static responses," *Journal of Engineering Mechanics*, vol. 137, no. 4, pp. 248–257, 2011.

[9] R. Ferrari, D. Froio, E. Rizzi, C. Gentile, and E. N. Chatzi, "Model updating of a historic concrete bridge by sensitivity- and global optimization-based Latin Hypercube Sampling," *Engineering Structures*, vol. 179, pp. 139–160, 2019.

[10] S. Weng, Y. Xia, Y. L. Xu, and H. P. Zhu, "Substructure based approach to finite element model updating," *Computers & Structures*, vol. 89, no. 9-10, pp. 772–782, 2011.

[11] O. Hasancebi and T. Dumlupınar, "Linear and nonlinear model updating of reinforced concrete T-beam bridges using artificial neural networks," *Computers & Structures*, vol. 119, pp. 1–11, 2013.

[12] Y. Xin, J. Li, H. Hao, N. Yang, and C. Li, "Time-varying system identification of precast segmental columns subjected to seismic excitations," *Journal of Bridge Engineering*, vol. 27, no. 4, Article ID 04022013, 2022.

[13] W. Tian, S. Weng, and Y. Xia, "Model updating of nonlinear structures using substructuring method," *Journal of Sound and Vibration*, vol. 521, Article ID 116719, 2022.

[14] F. M. Hemez and S. W. Doebling, "Review and assessment of modal updating for nonlinear, transient dynamics," *Mechanical Systems and Signal Processing*, vol. 15, no. 1, pp. 45–74, 2001.

[15] T. X. Zhu, G. B. Zhang, and C. P. Zang, "Frequency-domain nonlinear model updating based on analytical sensitivity and the Multi-Harmonic balance method," *Mechanical Systems and Signal Processing*, vol. 163, Article ID 108169, 2022.

[16] J. Shan, H. Zhang, W. Shi, and X. Lu, "Health monitoring and field-testing of high-rise buildings: a review," *Structural Concrete*, vol. 21, no. 4, pp. 1272–1285, 2020.

[17] J. P. Noel and G. Kerschen, "Nonlinear system identification in structural dynamics: 10 more years of progress," *Mechanical Systems and Signal Processing*, vol. 83, pp. 2–35, 2017.

[18] W. Song, S. J. Dyke, and T. Harmon, "Application of nonlinear model updating for a reinforced concrete shear wall," *Journal of Engineering Mechanics*, vol. 139, no. 5, pp. 635–649, 2013.

[19] E. Asgarieh, B. Moaveni, A. R. Barbosa, and E. Chatzi, "Nonlinear model calibration of a shear wall building using time and frequency data features," *Mechanical Systems and Signal Processing*, vol. 85, pp. 236–251, 2017.

[20] M. Kurt, K. J. Moore, M. Eriten, D. M. McFarland, L. A. Bergman, and A. F. Vakakis, "Nonlinear model updating applied to the IMAC XXXII Round Robin benchmark system," *Mechanical Systems and Signal Processing*, vol. 88, pp. 111–122, 2017.

[21] Z. C. Wang, Y. Xin, and W. X. Ren, "Nonlinear structural model updating based on instantaneous frequencies and amplitudes of the decomposed dynamic responses," *Engineering Structures*, vol. 100, pp. 189–200, 2015.

[22] Z. C. Wang, Y. Xin, and W. X. Ren, "Nonlinear structural joint model updating based on instantaneous characteristics of

dynamic responses," *Mechanical Systems and Signal Processing*, vol. 76-77, pp. 476–496, 2016.

[23] Y. Xin, H. Hao, J. Li, Z. C. Wang, H. P. Wan, and W. X. Ren, "Bayesian based nonlinear model updating using instantaneous characteristics of structural dynamic responses," *Engineering Structures*, vol. 183, pp. 459–474, 2019.

[24] R. Astroza, N. Barrientos, Y. Li, E. I. Saavedra Flores, and Z Liu, "Bayesian updating of complex nonlinear FE models with high-dimensional parameter space using heterogeneous measurements and a batch-recursive approach," *Engineering Structures*, vol. 201, Article ID 109724, 2019.

[25] J. Pal, S. Sikdar, and S. Banerjee, "A deep-learning approach for health monitoring of a steel frame structure with bolted connections," *Structural Control and Health Monitoring*, vol. 29, no. 2, Article ID e2873, 2021.

[26] C. Z. Dong and F. N. Catbas, "A review of computer vision-based structural health monitoring at local and global levels," *Structural Health Monitoring*, vol. 20, no. 2, pp. 692–743, 2020.

[27] S. Sony, S. Laventure, and A. Sadhu, "A literature review of next-generation smart sensing technology in structural health monitoring," *Structural Control and Health Monitoring*, vol. 26, no. 3, Article ID e2321, 2019.

[28] N. Bakhary, H. Hao, and A. J. Deeks, "Damage detection using artificial neural network with consideration of uncertainties," *Engineering Structures*, vol. 29, no. 11, pp. 2806–2815, 2007.

[29] Y. H. Guo, C. L. Du, Y. Zhao, T. F. Ting, and T. A. Rothfus, "Two-levelK-nearest neighbors approach for invasive plants detection and classification," *Applied Soft Computing*, vol. 108, Article ID 107523, 2021.

[30] R. Yu, P. Li, J. Shan, H. Zhu, C. N. Loong, and Z. Wei, "Multi-level deformation behavior monitoring of flexural structures via vision-based continuous boundary tracking: proof-of-concept study," *Measurement*, vol. 202, Article ID 111858, 2022.

[31] H. Z. Dai and Z. G. Cao, "A wavelet support vector machine-based neural network metamodel for structural reliability assessment," *Computer-Aided Civil and Infrastructure Engineering*, vol. 32, no. 4, pp. 344–357, 2017.

[32] G. Fan, J. Li, and H. Hao, "Vibration signal denoising for structural health monitoring by residual convolutional neural networks," *Measurement*, vol. 157, Article ID 107651, 2020.

[33] G. Fan, J. Li, H. Hao, and Y. Xin, "Data driven structural dynamic response reconstruction using segment based generative adversarial networks," *Engineering Structures*, vol. 234, Article ID 111970, 2021.

[34] I. Goodfellow, J. Pouget-Abadie, M. Mirza et al., "Generative adversarial nets," *Advances in Neural Information Processing Systems*, pp. 2672–2680, Montreal Canada, 2014.

[35] B. Zhao and Q. Yuan, "Improved generative adversarial network for vibration-based fault diagnosis with imbalanced data," *Measurement*, vol. 169, Article ID 108522, 2021.

[36] G. Fan, J. Li, and H. Hao, "Dynamic response reconstruction for structural health monitoring using densely connected convolutional networks," *Structural Health Monitoring*, vol. 20, no. 4, pp. 1373–1391, 2021.

[37] P. Isola, J. Y. Zhu, T. Zhou, and A. A. Efros, "Image-to-image translation with conditional adversarial networks," in *Proceedings of the 2017 IEEE Conference on Computer Vision and Pattern Recognition (CVPR)*, pp. 5967–5976, Beijing China, May 2017.

[38] X. Mao, C. Shen, and Y. B. Yang, "Immage restoration using very deep convolutional encoder-decoder networks with symmetric skip connections. Spain," *Advances in Neural Information Processing Systems*, pp. 2802–2810, Barcelona, 2016.

[39] C. S. N. Pathirage, J. Li, L. Li, H. Hao, W. Q. Liu, and R. H. Wang, "Development and application of a deep learning–based sparse autoencoder framework for structural damage identification," *Structural Health Monitoring*, vol. 18, no. 1, pp. 103–122, 2019.

[40] C. S. N. Pathirage, J. Li, L. Li, H. Hao, W. Q. Liu, and P. H. Ni, "Structural damage identification based on autoencoder neural networks and deep learning," *Engineering Structures*, vol. 172, pp. 13–28, 2018.

[41] A. Radford, L. Metz, and S. Chintala, "Unsupervised Representation Learning with Deep Convolutional Generative Adversarial Networks," in *Proceedings of the 9th International Conference, ICIG 2017*, Shanghai, China, September, 2017.

[42] D. Pathak, P. Krahenbuhl, J. Donahue, T. Darrell, and A. A. Efros, "Context encoders: feature learning by inpainting," in *Proceedings of the 2016 IEEE Conference on Computer Vision and Pattern Recognition (CVPR)*, pp. 2536–2544, Seoul Korea, June 2016.

[43] S. Mazzoni, M. H. Scott, F. Mckenna, G. L. Fenves, and L. Chen, *Open System for Earthquake Engineering Simulation-User Manual*p. 465p, University of California, Berkeley, California, 2006.

[44] Z. C. Wang, Y. Xin, J. F. Xing, and W. X. Ren, "Hilbert low-pass filter of non-stationary time sequence using analytical mode decomposition," *Journal of Vibration and Control*, vol. 23, no. 15, pp. 2444–2469, 2017.